Indian Geotech J (October 2020) 50(5):671–688
https://doi.org/10.1007/s40098-019-00405-2

ORIGINAL PAPER

Assessing and Updating Damage Probabilities for a Deep Excavation in Mexico City Soft Soils

C. J. Sainea-Vargas[1] · **M. C. Torres-Suárez**[2]

Received: 1 August 2019 / Accepted: 12 December 2019 / Published online: 20 December 2019

Abstract This paper presents the results of numerical and probabilistic modeling of a deep excavation in Mexico City soft soils, concerning the estimation of potential damages in neighboring buildings. Constitutive model hardening soil small strain was used to model soft soil behavior, and selected parameters E_0^{ref} and E_{50}^{ref} were represented as random variables and random fields. A combination of response surface method and random variable and random field-based tridimensional finite element modeling was employed to assess the excavation performance in terms of damage potential indexes. Results for the two representations of parameter spatial variability were obtained and compared for the different stages in the construction sequence. In the considered case, when uncertain parameters are modeled using highly anisotropic random fields, the assessed damage probability values differ considerably to the ones of random variable-based modeling. The distributions of calculated damage probabilities are also different for the buildings located around the excavation when changing the soil variability representation. On the other hand, calculated ground movements from semiempirical methods and actual measurements were integrated to obtain damage potential indexes for the excavation stages. The prior building damage probabilities and additional estimations are combined in a Bayesian framework to update the initial estimations. This approach allows also updating soil constitutive parameter values, resulting in equal prior and posterior mean values of parameters E_0^{ref} and E_{50}^{ref}, but reducing its uncertainty.

Keywords Bayesian updating · Building damage · Deep excavations · Numerical-probabilistic modeling · Random fields · Soft soils

Introduction

The design and construction of deep excavations in soft soils in urban areas are subjected to considerable difficulties, given its unfavorable mechanical behavior, which may generate structural damages during its execution [1]. Mexico City (CDMX) lacustrine zone imposes problematic conditions to geotechnical projects due to the presence of soft soils, materials of high compressibility and low shear strength, subjected to high-level water tables and regional subsidence related to water pumping in deep aquifers. The properties of these materials have been studied intensively since the second half of the twentieth century [2–4].

The lacustrine sediments in CDMX are complex mixtures of crystalline minerals and amorphous materials with microfossils content, which have unique properties [5]. These particular properties include a quite large natural water content, high plasticity, low undrained shear strength and very high compressibility; besides, there are dissolved minerals present in the pore water, and the regional consolidation process changes the soil compressibility with time [6]. As CDMX soils are naturally variable, recent efforts have been made to evaluate its spatial variability using geostatistical methods [3, 7, 8]. Excavation techniques in CDMX have evolved in the last decades [9], in parallel with the construction of important projects as the

✉ C. J. Sainea-Vargas
carlos.sainea@uptc.edu.co

[1] Escuela de Ingeniería Civil, Universidad Pedagógica y Tecnológica de Colombia, Avenida Central del Norte No. 39-115, Tunja, Boyacá, Colombia

[2] Facultad de Ingeniería, Universidad Nacional de Colombia, Av. NQS No. 45-03, Bogotá, Colombia

Latino Americana Tower which required one of 12 m depth [10] or the Mexico City Subway stations reaching 16 m in the downtown area [4, 11, 12]. Recently, top-down excavation process has become more common, and the excavation depths in CDMX have been increasing to depths beyond 30 m and more than 10 basement levels [13]. There are also recent regulations in which the design of the excavations must fulfill, including the ultimate and serviceability limit states requirements [14].

During the construction of deep urban excavations, damage assessment on neighboring buildings is needed [15, 16]. To appraise possible harms, the estimation of ground movements around deep excavations can be done through the use of numerical techniques as the finite element method. Constitutive model hardening soil small strain (HS-Small), an extension of hardening soil (HS) [17, 18] can be suitable for representing soft soil behavior for serviceability limit states analysis of deep excavations [19, 20]. As there are uncertainties involved in the damage assessment process, a combination of numerical and probabilistic techniques is convenient. In the numerical analyses, the constitutive soil parameters can be treated as random variables or as random fields, and the system response as a random variable to assess safety conditions in terms of probabilities of failure (Pf_i), damage or undesired performance probabilities (Pd_i) or reliability indexes (β) [21–25].

This paper presents an application of numerical and probabilistic analysis to an excavation project in CDMX, which involves 3D random variable and random field-based finite element analysis of a deep urban excavation in soft soils. The response of the modeled excavation is obtained in terms of building damage probabilities Pd_{ij} for building i and construction stage j, based on the damage potential index (DPI) [26, 27]. Available field and laboratory information from an actual project of deep excavation in CDMX soft soils were used, as well as vertical displacement measurements during construction [28]. Ground movements were also determined using semiempirical models KSJH [27] and KJHH [29], to calculate DPI values during excavation stages. The combination of prior $P'd_{ij}$, DPI values from *KJHH* and *KSJH* and actual measurements in a Bayesian framework permit updating the initial estimates.

Project Description

The excavation project is located in Paseo de la Reforma thoroughfare, next to the Angel of Independence monument roundabout, an iconic place in Mexico City. Major construction projects have been built recently in the same zone [13]. According to base information [28], the piece of land has an irregular shape and an area of 623.7 m^2. It was destined to the construction of a tower of 42 m height, 5 basement levels, ground floor and 12 levels.

The structure consists of steel and concrete columns, steel beams, concrete walls and reticular concrete slabs on the basement levels. Most of the project area was surrounded by an existing 0.6-m-thick diaphragm wall, which reaches 16.5 m depth, crowned by a concrete squared header beam with 1.0-m base. On the surface, there was a concrete slab with two holes for extracting excavated material, supported by the header beam, steel beams and steel columns supported by oblong concrete piles. Existing 0.6 × 2.7 m piles reaching 24 m below the street level were complemented using additional concrete piles with circular cross sections and varying lengths.

There was also an existing excavation until 2.5 m below the concrete slab level. The excavation for the parking basement reached a depth of 13.8 m including 0.8-m-thick bottom slab, and the excavation in the trapezium destined to the storm tank and cisterns attained 10.6 m depth. The project is adjacent to Paseo de la Reforma thoroughfare and Berna Street, and there were several buildings of different heights around the project, like a ground floor and 13-story building at the northwest side, 2- and 3-level houses at the south, a 5- and 7-story buildings at the west.

Geotechnical Conditions

The ground surface at the study site is nearly horizontal, and it is located on soft lacustrine soils belonging to geotechnical Zone III [3, 14]. Soils of Zone III are described as thick clay deposits, highly compressible, separated by sandy layers of medium to high relative density and variable thickness, with the presence of silts or clays [14].

Base information was taken from the geotechnical exploration carried out on soft lacustrine soils at the study site, which includes field and laboratory tests [28]. At the site one electric cone penetration test was performed to 31.7 m depth, standard penetration tests reached up 37.2 m depth, one observation tube was installed at 7.0 m, and four open piezometers at 11.5, 18.3, 22.4, and 27.5 m. A boring with sampling was also performed, obtaining 6 samples in soft soil strata using thin wall samplers. Laboratory consolidation and unconsolidated undrained triaxial test results were also performed.

Geotechnical Profile Description

The soils of interest in this research to be modeled as random variables and random fields are those of the upper clayey series locally named Formación Arcillosa Superior

(FAS) found between 5 and 22.2 m, and those of lower clayey series locally named Formación Arcillosa Inferior (FAI) found from 24.1 to 34.2 m depth.

- From 0.0 to 1.0 m, fill material composed by sandy silts with masonry and concrete debris.
- From 1.0 to 5.0 m, a superficial crust made up by natural materials including brown and gray silts and sandy silts, with an average cone tip resistance of 1180 kPa. On a sample obtained at 5.3 m from surface, classified as MH, it was found $w_n = 110\%$, $\gamma = 13.5$ kN/m^3, $c = 25$ kPa, $\phi = 24°$, $E_{50} = 7200$ kPa, $e_0 = 2.7$ and $\sigma_p = 230$ kPa.
- From 5.0 to 22.2 m, the upper clayey series (FAS) composed by clay layers separated by hard lenses composed by black basaltic sand, solar drying made up by dense sandy silts and silty sands and volcanic ashes. The average cone tip resistance in the clays is 620 kPa and in the hard lenses is between 2900 and 7800 kPa. On samples obtained at 8.4, 14.7 and 20.8 m from surface, classified as CH, it was found $284 < w_n < 391\%$, $11.3 < \gamma < 11.8$ kN/m^3, $44 < c < 82$ kPa, $0 < \phi < 5°$, $3300 < E_{50} < 10{,}000$ kPa, $6.7 < e_0 < 7.8$ and $90 < \sigma_p < 300$ kPa.
- From 22.2 to 24.1 m, a hard layer composed by sandy silt with clays and occasionally gravels, with varying cementation. Cone tip resistance for these materials is between 2900 and 9800 kPa.
- From 24.1 to 34.2 m, the lower clayey series (FAI) with the presence of hard lenses. Cone tip resistance in clays is between 980 and 2200 kPa and between 2900 and 5200 kPa in the hard lenses. On a sample obtained at 26.0 m from surface, classified as CH, it was found $w_n = 185\%$, $\gamma = 12.4$ kN/m^3, $c = 55$ kPa, $\phi = 11°$, $E_{50} = 9600$ kPa, $e_0 = 6.4$ and $\sigma_p = 380$ kPa.
- From 34.2 m, the deep deposits composed by sands and alluvial silty gravels cemented with hard clays and calcium carbonates. For these materials, the number of blows in SPT tests is beyond 50.

Piezometric Conditions

The observation tube and four open piezometers mentioned earlier allowed the determination of pore water pressures in the permeable lenses and obtaining effective stresses across all the geotechnical profile. The phreatic level is at 2.5 m depth, while at 11.5 m the pore pressure is 65 kPa, at 18.3 m is 82 kPa, at 22.4 m is 80 kPa and at 27.5 m is 88 kPa. These pressures were introduced as boundary conditions in the finite element models.

Soil Constitutive Model and Parameters

Constitutive model HS-Small [18], an extension of HS [17] to model soil behavior at small strains, is assumed as suitable to simulate soft soil behavior for the analysis of deep excavations [19, 20]. These are two constitutive models of isotropic hardening and two flow surfaces: one deviatoric surface with a nonassociated flow and one volumetric surface with an associated flow, where the Mohr–Coulomb failure criterion defines the ultimate limit state. These models allow the representation of aspects of the nonlinear behavior of the soil, including stiffness depending on the stress state, the effects of the history of stresses with the evolution of the preconsolidation pressure and different stiffness in loading and unloading [20].

In this research, the initial tangent modulus (E_0^{ref}) and the secant stiffness at 50% of the ultimate deviator stress at the reference minor principal stress (E_{50}^{ref}) were selected to be represented as random variables and random fields. The parameters in common for HS and HS-Small constitutive models are the elastic constants E_{50}^{ref}, $E_{\text{ur}}^{\text{ref}}$, υ_{ur}, reference stress σ^{ref}, stiffness exponent m, parameters for the shear mechanism c', ϕ', ψ, R_f, $e_{\max}$, f_t, D, for the volumetric cap mechanism $E_{\text{oed}}^{\text{ref}}$, $\sigma_{\text{oed}}^{\text{ref}}$, for stress history OCR, K_0^{SR} and parameters M, H for defining the shape of the yield surface and the rate of the plastic volumetric strain and the preconsolidation pressure. HS-Small model has two additional parameters: E_0^{ref} and $\gamma_{0.7}$.

Statistical Analyses

Parameter Decomposition

The spatial variability analysis supporting random field simulation relies on the stationarity assumption, at least of second order [30]. Aiming to fulfill the stationarity assumption, a usual procedure is to transform the data using techniques such as classical decomposition [31]. In classical decomposition, the spatial variability of any soil property $\xi(z)$ is divided into two parts: a known deterministic trend $t(z)$ and a zero mean, nonzero variance set of residuals expressing the soil parameter variation with respect to this trend, $w(z)$.

Descriptive and Inferential Analyses

Descriptive and inferential statistical analyses were performed on the residuals wE_{50}^{ref} and wE_0^{ref}, whose results are summarized in Table 1. In this table, n is the number of data points considered, $\bar{x}$ the mean value, s the standard deviation, C_s the skewness, C_k the kurtosis, *pdf* the fitted

Table 1 Descriptive and inferential analyses results for wE_{50}^{ref} and wE_{0}^{ref}

	wE_{50}^{ref} (kPa)	wE_{0}^{ref} (kPa)
n	286	286
$\bar{x}$	3.797E−8	− 2.022E−7
s	1031.151	6068.847
C_s	0.6788	0.5436
C_k	3.2985	2.7102
p value	0.259	0.066
pdf	I-Beta	I-Beta
Par1	3.0412	1.8231
Par2	11.2974	4.0162
Location	− 2091.6278	− 10,674.453
Scale	9861.654	34,189.963

probability density functions and *Par1*, *Par2*, *Location*, *Scale* their parameters. Pearson's type I-Beta pdfs were fitted using the first four sample statistical moments $\bar{x}$, s^2, C_s, C_k [22, 30]. Kolmogorov–Smirnov goodness of fit tests were used to check results, using a level of significance $\alpha = 0.05$. The selection of probability distributions and their parameters were made through the method of moments estimators and maximum likelihood estimation.

Spatial Statistical Analysis

Besides descriptive and inferential analyses on residuals of selected parameters, it is important to characterize their correlation structure for subsequent random field modeling. The scale of fluctuation (θ) is a measure of the variability in a random field, defined as the distance within which soil properties are significantly correlated, and it is an indicator of the spatial extension of the correlation structure [32]. In sedimentary soils, different scales of fluctuation are expected in vertical (θ_v) and horizontal (θ_h) directions caused by the deposition process. Some authors present θ values for geotechnical parameters [33, 34] and θ_h estimation using *CPT* data [35].

Fitting theoretical autocorrelation ($R_z(\delta)$) or variogram ($2\gamma(\delta)$) models to their particular sampling functions allow estimating θ [30, 32]. When fitting theoretical $R_z(\delta)$ or $2\gamma(\delta)$ models, θ is expressed as a function of the autocorrelation length of the former or the range of the latter [33, 36, 37]. Theoretical variogram models were fitted to empirically calculated sampling variograms for wE_{0}^{ref}, wE_{50}^{ref} and $wE_{0}^{ref} \cdot wE_{50}^{ref}$ to find θ_v values, using SGeMS v2.5b software [41]. There are several variogram theoretical models available as spherical (SPH), exponential (EXP) or Gaussian (GAU) [22, 30, 31, 38–40]. EXP variogram was fitted to sampling variogram and cross-variogram functions, as shown in Fig. 1. As wE_{0}^{ref} and wE_{50}^{ref} datasets were not univariate normal, they had to be transformed to normal scores [39, 40]. Table 2 summarizes the results of statistical spatial analyses for standardized residuals, where C_0 is the variogram nugget representing small-scale variability, $C_0 + C$ is the maximum value of variogram function known as the sill, and θ_v is the scale of fluctuation of the considered parameter in the vertical direction.

Random Field Simulation

A random function or random field (Z) is obtained by assigning a random variable to each space point. A regionalized variable (z) is a variable distributed in space that has a correlation structure which can not be known exhaustively, but only through a limited set of data as in this case wE_{0}^{ref} and wE_{50}^{ref}. Thus, Z would be a realization of z, although there could be many others with similar spatial distribution. Through geostatistical simulations, multiple artificial realizations Z_s can be obtained, reflecting the statistical properties of Z. Among all the possible simulations or artificial realizations, they are preferable all those in which the simulated values coincide with the experimental ones, called conditional simulations [21, 41].

Geostatistical methods for random field simulation include the sequential Gaussian simulation (SGSIM), the sequential Gaussian co-simulation (COSGSIM) and the direct sequential simulation (DSSIM) [39–41]. In this research, COSGSIM was chosen, previously converting data into Gaussian standard. Software SGeMS v2.5b [39] was used to generate random fields. In this case, given the geology of the study site and previous studies results [7, 8], it was assumed $a_r = 1000$. Figure 2 presents examples of simulated random fields for wE_{0}^{ref} and wE_{50}^{ref}.

Numerical Modeling

This section presents the general features of random field (RNDF) and random variable (RV)-based numerical models considered for assessing ground movements and potential damages in adjacent buildings to the considered deep excavation in CDMX soft soils.

Main Features of the Numerical Models

3D finite element models, as the ones presented in Figs. 3 and 4, were elaborated using ZSoil® v2016 software. The excavation is surrounded by buildings of different heights and shapes as listed in Table 3, and they were modeled as plates with distributed loads of 10 kPa per level. The project includes a building of 42 m height, 5 basement levels, ground floor and 12 levels. The excavation has an

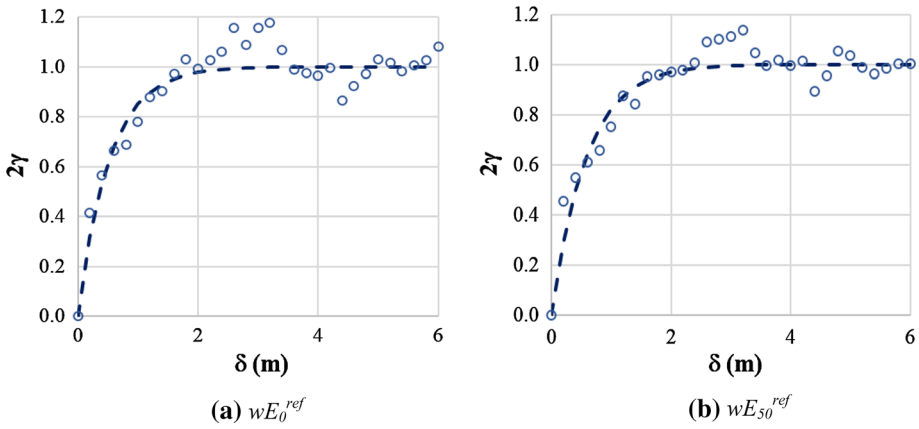

Fig. 1 Sampling and fitted theoretical variogram functions for standardized wE_0^{ref}, wE_{50}^{ref}

Table 2 Summary of θ_v obtained values from variogram functions for wE_0^{ref} and wE_{50}^{ref} transformed as Gaussian standard variables

Variable	C_0	$C_0 + C$	θ_v (m)
wE_0^{ref}	0	1	1.05
wE_{50}^{ref}	0	1	1.16
$wE_0^{ref} \cdot wE_{50}^{ref}$	0	0.93	1.07

irregular shape, whose dimensions are around 22.5 × 35 m and an area of 623.7 m^2.

Most of the excavation is destined to parking, but the zone adjacent to Paseo de la Reforma is for the boiler room, storm tanks and cisterns. The maximum excavation depth is 13.8 m in the parking basement zone and 10.6 m in the tank zone. Steel beams support the excavation in the parking basement, as well as 0.8-m-thick concrete bottom slab, existing concrete 0.30-m-thick existing slab and concrete beams on surface, concrete 0.15-m mezzanine slabs and the existing 0.6-m-thick and 16.5-m perimeter concrete diaphragm wall, crowned by a concrete squared header beam with 1.0-m base. In the boiler room, storm tank and cisterns, a soldier pile wall supported by steel beams and braces was used. Existing 0.6 × 2.7 m piles of 24 m depth were complemented using additional concrete piles with diameters between 0.6 and 1.20 m and different lengths: 17.5 m, 19.5 m, 21.0 and 22.0 m. Piles were modeled as beam elements embedded in the continuum. As they are embedded in the soil, soil pile interfaces were also created and a tip interface was included. Besides, pile head links were established in the contacts with the bottom plate.

The model extends to a 107.5 m × 122.5 m × 40 m block defined following recommendations found in the literature [42, 43]. Standard solid boundary conditions were defined on soil boundary box. Seepage elements were created in the contour faces of the model and on the faces representing the bottom of the excavation at each stage. These last ones were activated and deactivated depending on the construction sequence defined through existence functions in the modeling software. Fluid heads were created to represent phreatic level and pore water pressures in the permeable lenses. The initial stresses on bounding box were also defined. The faces of the excavation were defined as LE, LW, BN, BS, and a series of sections were established to extract the nodal displacements. Twenty pieces of land were defined to assess potential damages in buildings located around the excavation. Figure 3 and Table 3 present the nomenclature for the excavation faces and sections for analysis, as well as neighboring building numbering. Models elaborated have a total of 79,872 hexahedral B8 elements and 88,414 nodes, with 63,210 finite elements in the soft soil layers whose selected parameter values were simulated as random.

The numerical simulations focus on the construction phase of the project and do not consider long-term effects. As the construction is thought as occurring in a relatively short time, and the soils have low permeability, and undrained conditions were assumed with analysis in terms of effective stresses rather than performing coupled deformation analyses that would suppose a much higher computational cost. The modeling of changes in the groundwater level is done considering the changes in the drainage boundaries in each stage of construction as wall installation, excavation of a given soil volume or bottom plate installation and solving a permanent flow problem. In the next step, the pressure fields found for each stage are assigned as inputs to the mechanical problem using the effective stress principle. The stages in considered construction sequence are listed in Table 4.

Table 5 summarizes constitutive parameter values used in numerical modeling. A geotechnical model composed of thirty-six layers was defined in which layer L1 corresponds to a fill layer, CS the superficial crust and CD the deep deposits whose properties were considered as deterministic. Layers L4 to L23 and L26 to L35 are the soft soil layers modeled from random fields for the selected parameters. Other assumed soil parameter values are f_t = 0 kPa,

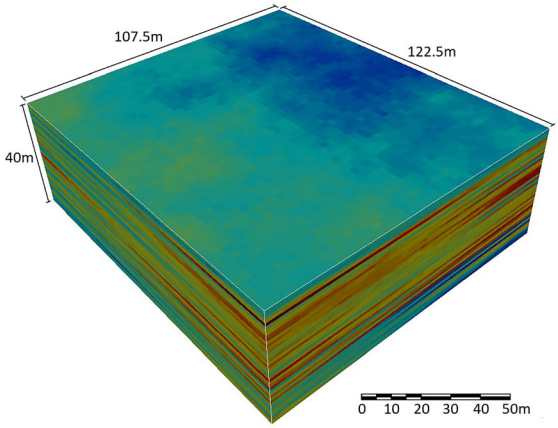

(a) *RNDF* for wE_0^{ref}

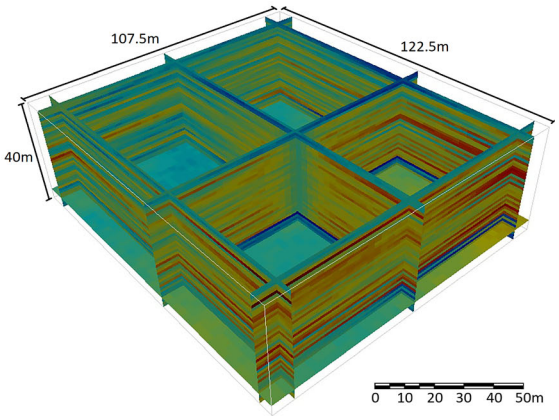

(b) Cross-sections in *RNDF* for wE_0^{ref}

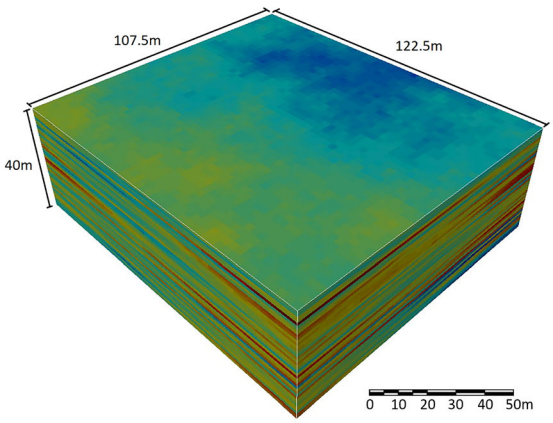

(c) *RNDF* for wE_{50}^{ref}

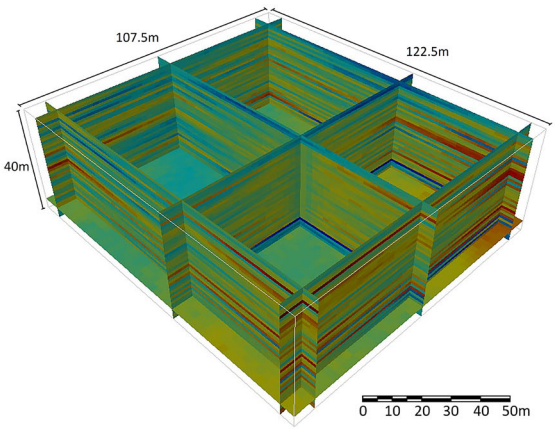

(d) Cross-sections in *RNDF* for wE_{50}^{ref}

Fig. 2 Simulated random fields for wE_0^{ref} and wE_{50}^{ref}

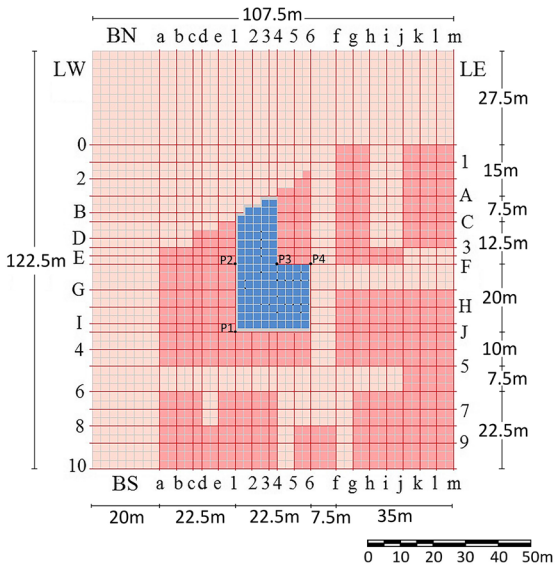

(a) Finite element model and sections for *DPI* determination

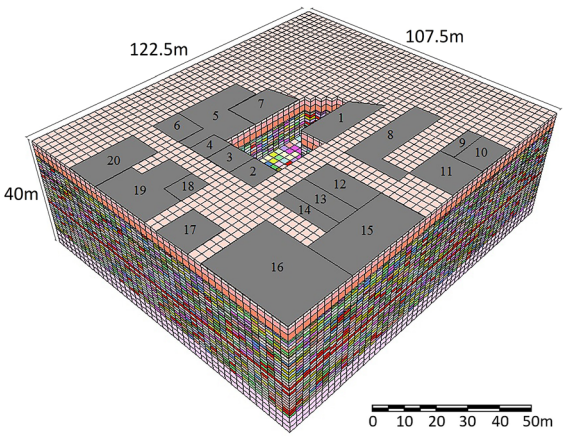

(b) 3D random field-based finite element model showing nearby building areas

Fig. 3 Sections for DPI determination and building areas for Pd_{ij} assessment

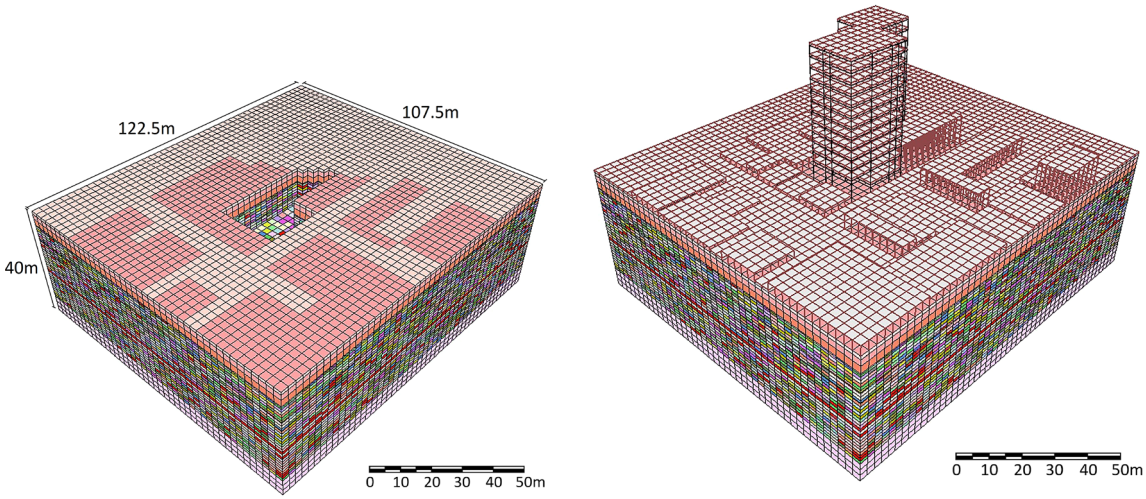

(a) Random field-based finite element model showing the excavation and surrounding plates

(b) Random field-based finite element model including the building and surrounding loads

Fig. 4 Random field-based deep excavation in soft soils 3D FEM model

Table 3 Number of levels in buildings and sections for DPI calculation

Building	Number of levels	Excavation face	Sections for DPI calculation
1	14	LE, BN	2, A, B, C, D, 3, E, F, 4, 5, 6
2	4	BS	4, 5, 6
3	2	BS	2, 3, 4
4	3	BS	e, 1
5	5	LW	3, E, F, G, H, I, J, 4, 5
6	3	LW	J, 4, 5
7	7	LW	C, D, 3, E, F, G
8	9	LE	0, 1, 2, A, B, C, D, 3, E, F
9	4	LE	0, 1, 2, A
10	14	LE	0, 1, 2, A
11	2	LE	A, B, C, D, 3
12	2	LE	G, H, I
13	5	LE	I, J, 4
14	7	LE	4, 5
15	3	LE	G, H, I, J, 4, 5, 6
16	4	BS	g, h, i, j, k, l, m
17	4	BS	5, 6, f
18	1	BS	2, 3, 4
19	2	BS	d, e, 1, 2, 3, 4
20	3	BS	a, b, c, d

$\psi = 12°$, $\gamma_{0.7} = 0.00025$ for the fill layer, $f_t = 0$ kPa, $\psi = 13.85°$, $\gamma_{0.7} = 0.0001$ for CS, $f_t = 0$ kPa, $\psi = 10°$, $\gamma_{0.7} = 0.0001$ for CD, $f_t = 0$ kPa, $\psi = 0°$, $\gamma_{0.7} = 0.0055$ for the remaining ones. Besides, $\upsilon_{ur} = 0.20$, $m = 0.8$, $\sigma_{ref} = 100$ kPa, $R_f = 0.9$, $D = 0.25$.

DPI

As the response variable, the damage potential index (DPI) was chosen [26, 27]. DPI is based on the maximum principal tensile strain (ε_P) originated by excavation in adjacent buildings which combines angular distortion (β), lateral deformation (ε_L) and the direction of crack formation measured from vertical plane α_{max} [44].

Main Features of the Random Field-Based Numerical Models

The simulated random fields were discretized, added to initially removed trend values and mapped to the finite element mesh. A total of 13,746 materials were created to include soil properties for the numerical models, including the combinations of parameters from random fields. The aspect of a random field-based finite element model is presented in Fig. 4. The dimensions for each finite continuum element are 1 × 2.5 × 2.5 m.

Semiempirical Models KJHH and KSJH

KHJJ is a semiempirical model useful to predict the maximum wall deflection, maximum surface settlement and surface settlement profile related to braced excavations in clay [29]. It was developed based on FEM analysis results, considering nonlinear stress–strain behavior of clays at small strain levels. The model consists of three submodels: Model A given for predicting maximum wall deflection (δ_{hm}), Model B for predicting the deformation ratio (R) and maximum vertical surface settlement (δ_{vm}), respectively,

Table 4 Construction sequence considered in numerical analyses

Stage	Construction activities	Stage	Construction activities
1	New piles, columns, soldier wall	8	Fourth-level beams and slab (− 8.0 m)
2	Remaining first-level beams (0.0 m)	9	Excavation 4 (− 8.0 m to − 10.6 m)
3	Excavation 1 (− 2.5 to − 2.8 m)	10	Fifth-level beams and slab (− 10.6 m)
4	Second-level beams and slab (− 2.8 m)	11	Excavation 5 (− 10.6 to − 13.8 m)
5	Excavation 2 (− 2.8 to − 5.4 m)	12	Bottom slab
6	Third-level beams and slab (− 5.4 m)	13	Head beam demolition
7	Excavation 3 (− 5.4 to − 8.0 m)	14	Building construction

Table 5 Soil constitutive parameters employed in numerical analyses

Layer	σ_{oed}^{ref} (kPa)	k_0	e_{max}	M	H	γ (kN/m^3)	c' (kPa)	ϕ' (°)	E_{50}^{ref} (kPa)	E_{ur}^{ref} (kPa)	E_{oed}^{ref} (kPa)	E_0^{ref} (kPa)	OCR
Fill	242.59	0.412	2.06	1.29	8610.49	14.00	10.00	36.00	20,000	80,000	14,000	97,637	4.00
CS	296.98	0.337	1.97	1.43	14,016.69	14.10	1.65	41.55	22,841	68,522	22841	93,129	2.58
CS	296.98	0.337	1.95	1.43	14,016.69	14.10	1.65	41.55	22,841	68,522	22,841	93,129	2.58
L4	288.25	0.347	6.49	1.36	950.39	11.04	1.97	40.77	2453	7360	1717	21,018	2.40
L5	285.31	0.350	6.43	1.35	949.93	11.09	2.11	40.50	2426	7279	1698	21,233	2.34
L6	281.23	0.356	7.39	1.34	949.58	11.16	2.31	40.12	2388	7166	1672	21,546	2.26
L7	276.92	0.361	5.73	1.33	949.08	11.24	2.55	39.71	2348	7044	1644	21,892	2.17
L8	273.29	0.366	4.28	1.32	947.73	11.30	2.78	39.35	2313	6939	1619	22,199	2.10
L9	270.14	0.370	4.52	1.31	947.32	11.36	3.01	39.04	2282	6847	1598	22,475	2.04
L10	267.91	0.373	5.95	1.31	946.15	11.41	3.18	38.81	2260	6781	1582	22,678	1.99
L11	266.62	0.375	5.15	1.30	945.74	11.43	3.29	38.68	2247	6743	1573	22,798	1.97
L12	264.93	0.377	4.35	1.30	945.04	11.46	3.44	38.50	2231	6692	1561	22,958	1.93
L13	262.73	0.381	4.74	1.29	944.77	11.51	3.65	38.27	2208	6626	1546	23172	1.89
L14	260.92	0.383	6.36	1.29	944.06	11.55	3.83	38.08	2190	6571	1533	23,352	1.85
L15	259.99	0.385	4.85	1.29	943.48	11.57	3.93	37.98	2181	6542	1526	23,447	1.84
L16	258.92	0.386	5.06	1.28	943.54	11.59	4.04	37.86	2170	6509	1519	23,558	1.81
L17	257.24	0.389	4.76	1.28	943.22	11.63	4.24	37.68	2152	6457	1507	23,733	1.78
L18	255.70	0.391	4.40	1.27	941.99	11.66	4.43	37.51	2136	6409	1495	23,899	1.75
L19	254.27	0.393	5.64	1.27	941.86	11.70	4.61	37.35	2121	6364	1485	24,056	1.72
L20	252.93	0.395	6.88	1.27	941.33	11.73	4.80	37.20	2107	6321	1475	24,205	1.70
L21	251.68	0.397	5.08	1.26	941.01	11.76	4.97	37.06	2094	6282	1466	24,347	1.67
L22	250.50	0.399	3.28	1.26	940.43	11.78	5.15	36.93	2081	6244	1457	24,483	1.65
L23	249.40	0.401	5.36	1.26	940.30	11.81	5.33	36.80	2069	6209	1449	24,613	1.63
CD	272.67	0.367	1.65	1.42	9222.76	16.00	8.90	39.29	12,899	38,698	12,899	97,637	2.41
CD	272.67	0.367	1.65	1.42	9222.76	16.00	8.90	39.29	12,899	38,698	12,899	97,637	2.41
L26	246.52	0.406	5.36	1.25	938.99	11.88	5.82	36.47	2038	6115	1427	24,962	1.57
L27	245.53	0.407	5.34	1.24	938.15	11.91	6.00	36.35	2028	6083	1419	25,084	1.55
L28	244.68	0.409	5.32	1.24	938.30	11.93	6.16	36.25	2018	6055	1413	25,192	1.54
L29	243.86	0.410	5.29	1.24	938.26	11.95	6.33	36.15	2009	6028	1407	25,296	1.52
L30	243.08	0.411	5.20	1.24	937.99	11.97	6.49	36.06	2001	6002	1401	25,397	1.51
L31	242.33	0.413	5.19	1.23	937.46	11.99	6.64	35.97	1993	5978	1395	25,494	1.49
L32	241.62	0.414	5.18	1.23	936.85	12.01	6.80	35.88	1985	5954	1389	25,589	1.48
L33	240.93	0.415	5.17	1.23	936.95	12.03	6.96	35.80	1977	5931	1384	25,681	1.47
L34	240.93	0.415	5.17	1.23	936.95	12.03	6.96	35.80	1977	5931	1384	25,681	1.47
L35	240.93	0.415	5.17	1.23	936.95	12.03	6.96	35.80	1977	5931	1384	25,681	1.47
CD	272.66	0.367	1.65	1.42	9212.19	16.00	8.90	39.29	12,889	38,698	12,889	97,637	2.41

and Model C for predicting the surface settlement profile. On the other hand, KSJH is another semiempirical model, similar and complementary to KJHH model, useful to estimate lateral ground movement [27].

Methods for Probabilistic Analyses

Prior Probabilistic Analysis

Regarding prior probabilistic analyses, some authors explain different methodologies for carrying out reliability analysis in geotechnical applications [22–25, 45, 46]. RSM [47, 48] and PEM [21, 22, 24, 32, 49] were selected for prior probabilistic analyses.

Response Surface Method (RSM)

Assuming the response of a variable of interest Y as dependent on a set of variables $X_1, \ldots, X_k$, a functional relationship $Y = f(X_1, \ldots, X_k) + \varepsilon$ may be unknown. The form of function f is unknown, and the term ε represents other sources of variability not contemplated and is treated as a statistical error [48]. If $\mu_\varepsilon = 0$, the expected response is $E(Y) = f(X_1,\ldots, X_k) \equiv \eta$, the response surface. The function can be approximated by a polynomial of first or second order without cross-terms as in Eq. 1, as commonly used in *RSM* applications [47]. Least squares method, equating values of performance function and values of the polynomial equation evaluated at selected points, allows finding the coefficients β_i of polynomial equations. Once calculated β_i values, the subsequent analysis uses the fitted response surface.

$$y = f(x_1, x_2, \ldots, x_k) = \beta_0 + \sum_{i=1}^{k} \beta_i x_i + \sum_{i=1}^{k} \beta_{ii} x_i^2 \tag{1}$$

Y is evaluated around a center point defined by input variables mean values $\{x_{c1}, x_{c2}, \ldots, x_{ck}\}$, and other $2\,k$ points around it: $\{x_{c1} \pm m_p\sigma x_1, x_{c2} \ldots, x_{ck}\}$, $\{x_{c1}, x_{c2} \pm m_p\sigma x_2, \ldots, x_{ck}\},\ldots,\{x_{c1}, x_{c2}, \ldots, x_{ck} \pm m_p\sigma x_k\}$, where m_p is a parameter determining the relative distance of points for sampling. In this research, $m_p = 1$ was assumed to make results comparable with those of PEM and to avoid finding negative values for the constitutive parameters. Fitted response surface can be used to estimate statistical moments of distribution using MCS [50] or finding β using FORM [51, 52].

Point Estimation Method (PEM)

This method serves to estimate the moments of the performance function by evaluating it in a series of discrete selected points [21, 49]. PEM seeks to replace a continuum *pdf* with a discrete function having the same first three central moments. It does not require knowing the distribution function of the individual variables or the joint *pdf*. PEM application starts from a function of random variables $Y = f(X_1, X_2, \ldots, X_n)$ and known values of their means μ_{xi} and standard deviations σ_{xi} at 2^n points of interest. An initial point is located at mean values of all variables $y_{0} = f(\mu_{x1}, \mu_{x2},\ldots, \mu_{xn})$, and the others are defined such that the value of each variable is a standard deviation above or under its mean as $y_i^+ = f(\mu_{x1}, \mu_{x2},\ldots, \mu_{xi} + \sigma_{xi},\ldots, \mu_{xn})$ and $y_i^- = f(\mu_{x1}, \mu_{x2},\ldots, \mu_{xi}-\sigma_{xi},\ldots, \mu_{xn})$. A variant of this method considers $2n + 1$ points and obtaining Y mean and variance as expressed in Eqs. 2 and 3 [24, 53].

$$\bar{Y} = y_0 \prod_{i=1}^{n} \left[1/2(y_i^+ + y_i^-)/y_0)\right] \tag{2}$$

$$V_Y = \left\{ \left[\prod_{i=1}^{n} \left(1 + \left[y_i^+ - y_i^-/y_i^+ + y_i^-\right]^2\right)\right] - 1 \right\}^{1/2} \tag{3}$$

Damage Probability Assessment

A limit state function must be defined to assess the probability of undesired performance. For serviceability limit states related to possible cracking in adjacent buildings to the excavation, the limit state function is expressed as a margin of safety in Eq. 4, where R, DPI_R represent the capacity or resistance of the system and Q, DPI_L the loads or solicitations imposed. For reliability analysis, $\mathrm{DPI}_R = 23.8c_1$ based on a tensile limit strain $\varepsilon_p = 1.19 \times 10^{-3}$ is assumed, where c_1 is a bias factor [54]. DPI_L values were found from nodal displacements in numerical analyses for each section shown in Fig. 3.

$$M = R - Q = \mathrm{DPI}_R - \mathrm{DPI}_L \tag{4}$$

If $M > 0$ the excavation performance is satisfactory for the serviceability limit state defined, and if $M \leq 0$ there is a condition of undesired behavior, in this case implying cracking in adjacent buildings. Damage probability in each building and construction stage Pd_{ij} is obtained integrating the joint probability density function $f(\underline{x})$ over the misperformance region. When applying RSM, 10^5 Monte Carlo simulations were carried out using polynomial equations to find the first two statistical moments of M and Eqs. 2 and 3 when using PEM. The first two statistical moments of the limit state functions were used to solve Eq. 5 for appraising damage probabilities in each building and construction stage considered, for models based on random variables and random fields.

$$P_{di} = P[M(\underline{X}) \leq 0] = \int_{M(X) \leq 0} f(\underline{x}) \mathrm{d}x_1, \mathrm{d}x_2, \ldots, \mathrm{d}x_n \quad (5)$$

Bayesian Updating

Analytical and numerical initial predictions achieved are not perfect, given limitations in knowledge in each step of the prediction process. Some errors occur when transforming field and laboratory data into soil parameters, and others appear because of simplifications made when modeling real problems, for example, in boundary conditions and constitutive laws for materials behavior. In geotechnical engineering, in the framework of the observational method, Bayesian updating is a helpful tool to enhance predictions combining information from different sources [55–59]. Bayes' rule in Eq. 6 defines the updating of a prior probability $P'(x_j)$ to a posterior probability $P''(x_j|z_i)$ when new data z_i from another source are available.

$$P''(x_j|z_i) = \left[P(z_i|x_j)P'(x_j)\right] / \left[\sum (z_i|x_j)P'(x_j)\right] \quad (6)$$

The numerator in Eq. 6 contains the likelihood $P(z_i|x_j)$ and prior probability $P'(x_j)$, both related to a specific value of x_j. The denominator refers to the evidence related to all x_j possible values, and in the case of continuous variables, the sum becomes an integral. Often posterior probability is expressed for random variables as in Eq. 7, where k is a normalizing constant to ensure posterior probability integrating to 1. In this research, numerically assessed $\mathrm{DPI}_{Lij}(x)$ *pdf* updating for building i and excavation stage j is performed using $\mathrm{DPI}_{Lij(KJHH,\ KSJH)}$ values obtained from ground movements assessed using semiempirical models *KSJH* [27] and *KJHH* [29]. Equation 8 expresses the likelihood function assuming a multiplicative error ε_{ij} with a Gaussian distribution.

$$f_X''(x) = kL(x)f_X'(x) \quad (7)$$

$$\begin{aligned} L_{ij}(x) &= f\varepsilon_{ij}\left(DPI_{Lij(KJHH,KSJH)}/DPI_{Lij}(x)\right) \\ &= N\left(DPI_{Lij(KJHH,KSJH)}/DPI_{Lij}(x)\right) \end{aligned} \quad (8)$$

The difficulties in Bayesian updating arise when trying to solve the integral to find k, as analytical solutions are available only for the so-called conjugate priors [57]. The use of Markov chain Monte Carlo (*MCMC*) methods is common because they allow direct sampling from the posterior distribution without the need for solving integrals and computing k. As the application of such methods is computationally demanding, in this research, OpenBUGS v3.2.3 was the tool selected to perform Bayesian updating analyses.

Prior Probabilistic Analyses Results

This section presents the assessed damage probabilities Pd_{ij} for each building i and construction stage j. Different aspects are considered for results comparison: a validation of results taking into account the probability distribution of random parameters $X_1,\ldots, X_k$ in *RSM*, Gaussian or Pearson's type I-Beta, the method employed for Pd_{ij} assessment, *RSM* or *PEM*, and soil parameter representation, random fields (RNDF) or random variables (RV).

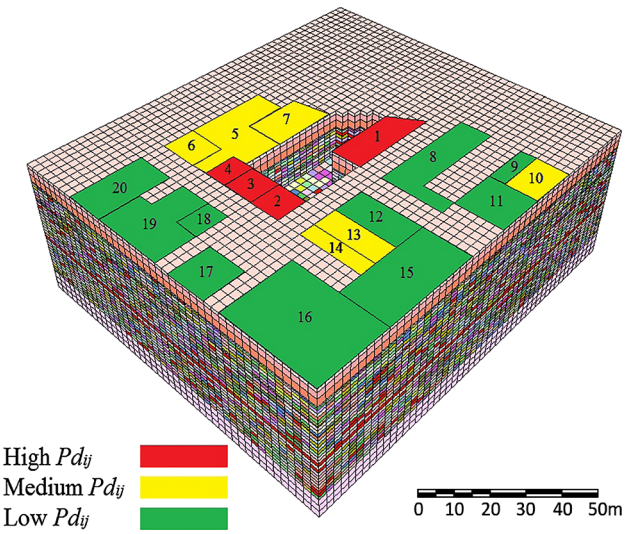

Fig. 5 Qualitative distribution of assessed Pd_{ij} values in RNDF-based models when using *RSM* and Gaussian random variables

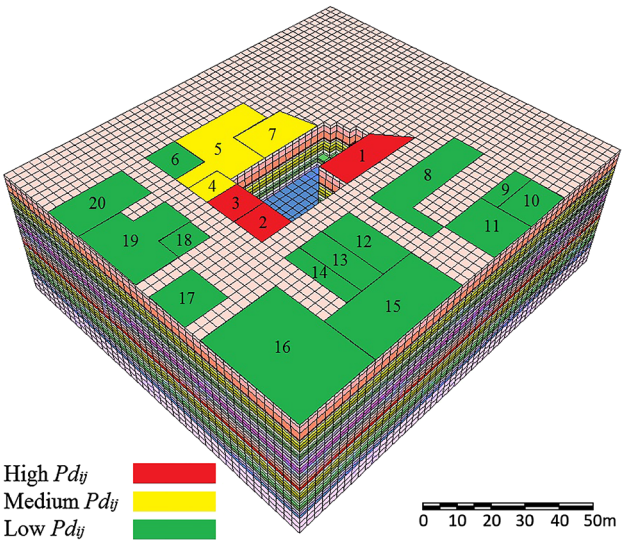

Fig. 6 Qualitative distribution of assessed Pd_{ij} values in RV-based models when using RSM and Gaussian random variables

Qualitative Damage Distribution

Figures 5 and 6 portray a qualitative distribution of assessed Pd_{ij} values when using RNDF and RV-based models and *RSM* with Gaussian random variables, respectively. The distribution in both cases is similar, but higher Pd_{ij} values were found for RNDF-based models.

Soil Parameter Representation, RNDF or RV

Figure 7 summarizes the assessed Pd_{ij} values obtained for RNDF and RV-based models using *RSM* and Gaussian random variables. The graphs have similar trends in both cases, but assessed damage probabilities are much higher for RNDF-based models. Pd_{ij} values can be compared with target values from the literature to appraise the excavation performance [60]. Considering all buildings and constructions stages simulated, a total of 280 cases were analyzed; 83.9% are above average ($0.001 < Pd_{ij} < 0.006$) or better, 16.1% are below average ($0.006 < Pd_{ij} < 0.023$) or worse when using RNDF, and 95.4% are above average or better, 4.6% are below average or worse when using RV.

When considering each building separately for RNDF-based models, B6, B8, B11, B12, B15, B16, B17, B18,

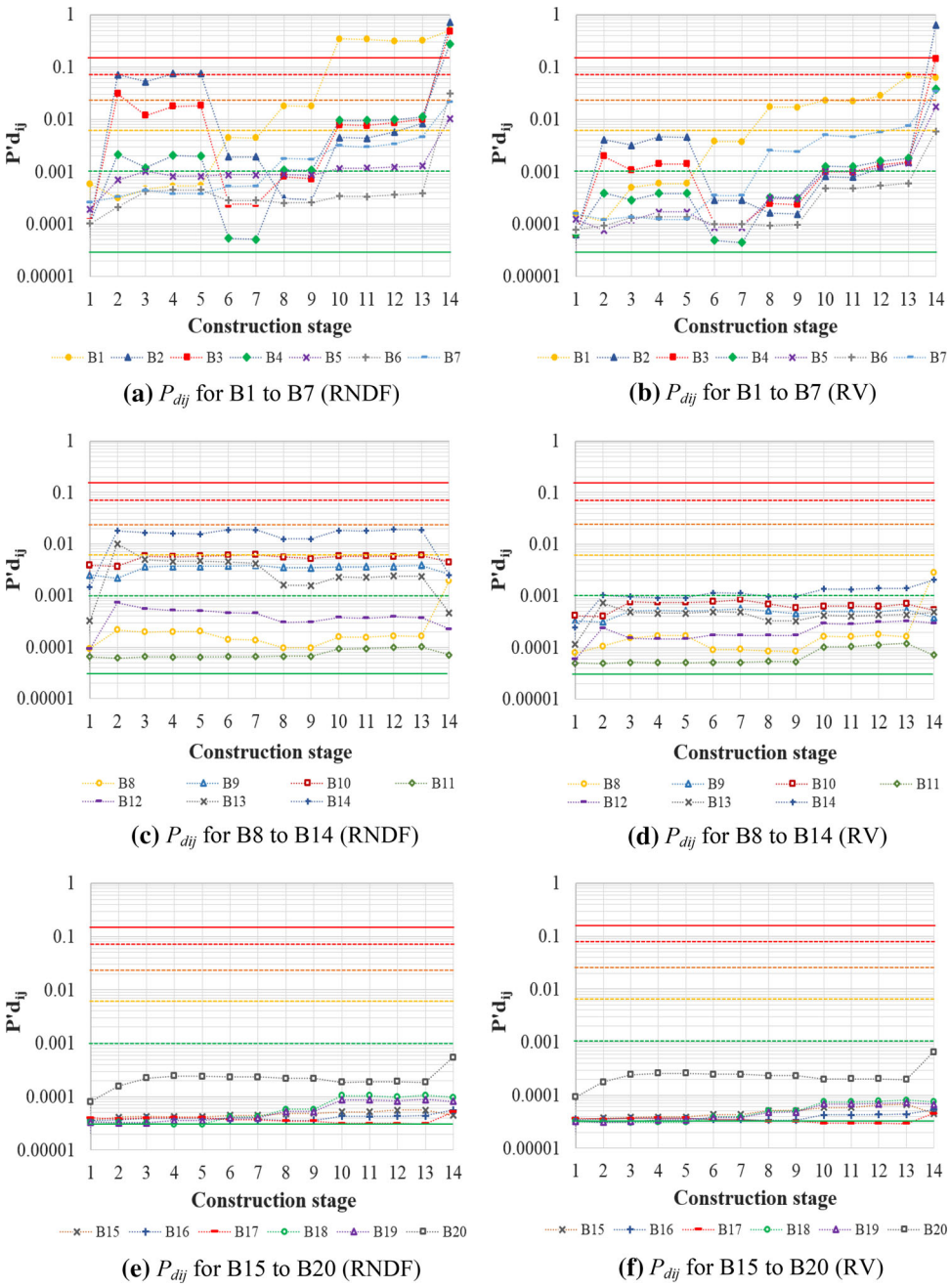

Fig. 7 Assessed P_{dij} values using RSM and Gaussian random variables

(a) P_{dij} for B1 to B7 (RNDF)

(b) P_{dij} for B1 to B7 (RV)

(c) P_{dij} for B8 to B14 (RNDF)

(d) P_{dij} for B8 to B14 (RV)

(e) P_{dij} for B15 to B20 (RNDF)

(f) P_{dij} for B15 to B20 (RV)

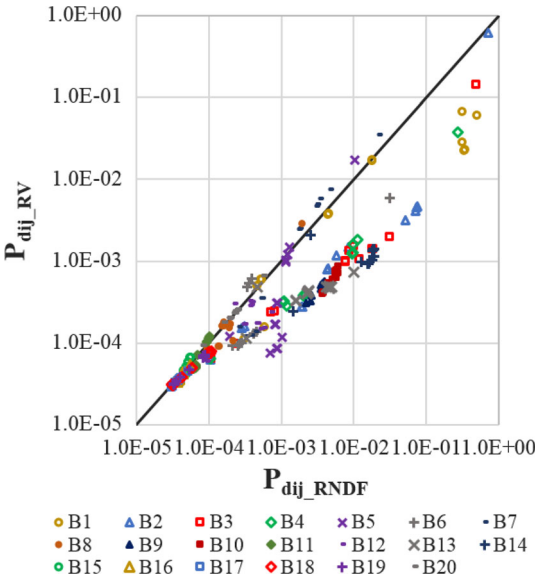

Fig. 8 Comparison of assessed P_{dij} values using RSM in RNDF and RV-based models

B19, B20 have a good performance ($0.001 < Pd_{ij} < 0.00003$) in at least 92.9% of the cases, and B5, B7, at least in 50%. In B9, 100% and in B10, B13 at least 78.6% of the cases are above average ($0.001 < Pd_{ij} < 0.006$). In B14, 85.7% of the cases are below average ($0.006 < Pd_{ij} < 0.023$), and in B3, 50% are below average, 7.1% have poor performance ($0.023 < Pd_i < 0.07$), and 7.1% presented a hazardous performance ($Pd_{ij} > 0.16$). In B4, 28.6% are below average, and 7.1% have a hazardous performance. In B2, 7.1% of the cases are below average, 7.1% have a poor performance, 21.4% are unsatisfactory, and 7.1% are hazardous. Finally, the most unfavorable condition occurs in B1, where 14.3% are below average, and 35.7% have a hazardous performance.

Figure 8 presents a comparison of assessed Pd_{ij} values using *RSM*, comparing results for RNDF and RV-based models. In general, data points separate from the 1:1 line, and when considering results for all buildings, the differences in assessed Pd_{ij} values are around 60%. When considering separately the results for each building, the differences in assessed Pd_{ij} are under 10% for B7, B8, B11, B15, B16, B17, B19, B20. The differences are between 10 and 50% for B2, B3, B4, B13, B18, and over 50% for B1, B5, B6, B9, B10, B11, B12, B14, B18. Given the results presented in this section, it is clear that in the case of the random field with assumed anisotropy ratio, the obtained results are not equivalent to those from random variable-based models. The performed predictions for RV-based models are in most of the cases under the ones obtained using RNDF-based models.

Random Variable Distribution in RSM, Gaussian or Beta

Figure 9 presents a comparison of assessed Pd_{ij} values for the random field and random variable-based models using *RSM* when considering Gaussian and Pearson's type I-Beta probability distributions for random parameters $X_1, \ldots, X_k$. The Pd_{ij} results obtained in both cases are similar; when considering results for all buildings, the differences in Pd_{ij} are on average around 25% for RNDF and 6% for RV-based models. When considering separately the results for each building, the differences in assessed Pd_{ij} are under 10% for all RV models and B8, B11, B15, B16, B17 in RNDF models. They are between 10 and 20% for B7, B12, B18, B19, B20, between 20 and 50% for B1, B2, B3, B4, B5, B6 and between 50 and 70% for B9, B10, B13, B14 in RNDF models. Results for RNDF models indicate slightly higher Pd_{ij} values when using Beta distributions and equivalent results for RV models.

Probabilistic Method, RSM or PEM

Figure 10 presents a comparison of assessed Pd_{ij} for the random field and random variable-based models using Gaussian distribution for random parameters when considering *RSM* and *PEM* methods. The Pd_{ij} values found by these two methods are also similar, as in the previous case; when considering results for all buildings, the differences in Pd_{ij} are on average around 14% for RNDF and 2% for RV-based models. When considering separately the results for each building, the differences in assessed Pd_{ij} are under 10% for most of the RV models and B8, B11, B15, B16, B17, B18, B19 in RNDF models. They are between 10 and 20% for B2, B3 in RV models and for B1, B6, B12 in RNDF models. They are between 20 and 50% for B2, B3, B5, B7, B9, B10, B13, B14, B20 and over 50% for B4 in RNDF models. Results for RNDF models deliver slightly higher Pd_{ij} values when using *RSM* and equivalent results for RV models.

Bayesian Updating of Initial Performance Predictions

For damage probability assessment, the limit state function is expressed as a margin of safety in Eq. 4. The Bayesian updating is given in terms of DPI_L, using calculated values for RNDF-based models and the *RSM* method. The numerically assessed mean values of $DPI_{Lij}(x)$ were updated for each building i and excavation stage j using values from measured vertical displacements and semiempirical models *KSJH* and *KJHH*, $DPI_{Lij(Meas,\ KJHH,\ KSJH)}$. Measured vertical displacements in monitoring points P1 to P4 of Fig. 3, presented in Fig. 11,

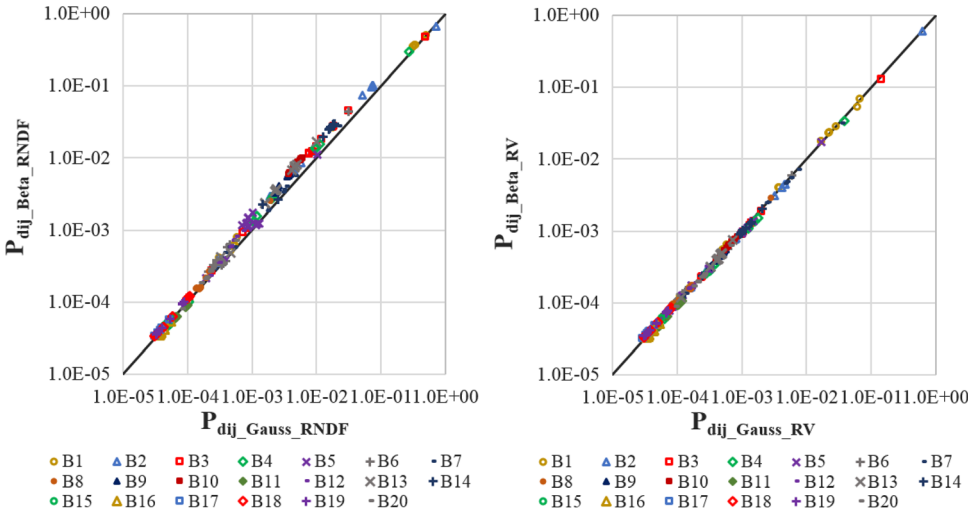

(a) P_{dij}, RNDF **(b)** P_{dij}, RV

Fig. 9 Comparison of assessed P_{dij} values for RNDF and RV-based models, using RSM and considering Gaussian and Beta probability distributions

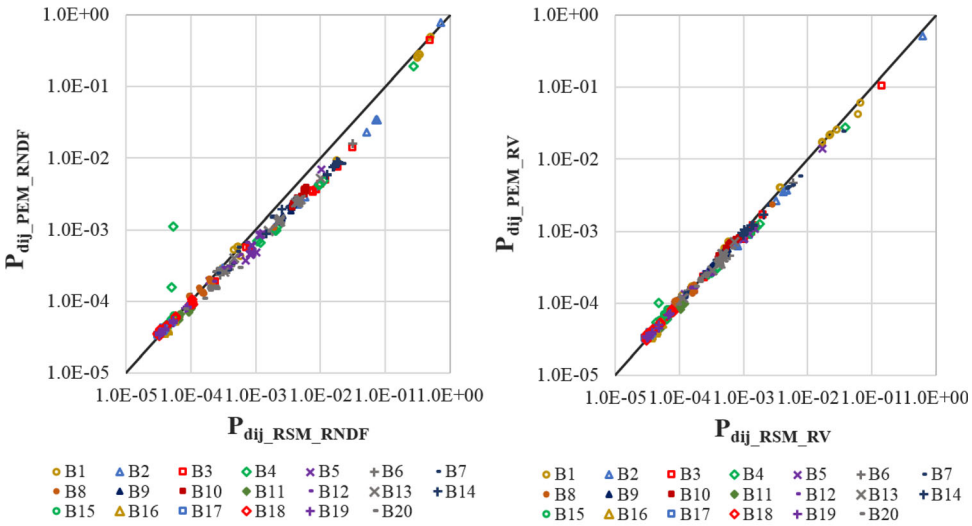

(a) P_{dij}, RNDF **(b)** P_{dij}, RV

Fig. 10 Comparison of assessed P_{dij} values for RNDF and RV-based models, using RSM and *PEM*

were employed to correct the ones obtained through *KJHH*. The distributions of both lateral and vertical ground displacements as a function of maximum values were assessed through an existing approach [43]. The estimated and corrected ground movements were used to compute the $\mathrm{DPI}_{Lij(Meas,\ KJHH,\ KSJH)}$ values presented in Fig. 11.

Bayesian updating was performed through *MCMC* employing OpenBUGS v3.2.3 software, which uses the Metropolis–Hastings algorithm and its special case Gibbs sampling [61, 62]. In the sample from the posterior distribution in *MCMC*, the values in the chain must be representative of the posterior distribution, and the chain should have the sufficient size to allow obtaining accurate and stable estimates [62]. Three chains were generated by starting a Metropolis–Hastings algorithm at different initial values, and a total of 20,000 simulations were generated for each chain, discarding the initial 2000 as burn-in samples to obtain the convergence of the chains and stable estimates.

The prior model is based on the polynomial equations from *RSM* for each building and construction stage. The polynomial equation is a function of E_0^{ref} and E_{50}^{ref}, assumed as Gaussian with standard deviations given in Table 1 and mean value for each layer given in Table 5. The coefficients β_i of the polynomial equations are the same used in the previous sections for the selected model series. Figure 12 presents a comparison of $\mathrm{DPI}_{Lij(KJHH\text{-}KSJH)}$ and mean values of $\mathrm{DPI}_{Lij}(x)$ assessed from nodal displacements obtained in numerical and probabilistic analyses. The first method, which includes actual measurements of vertical displacements to correct the ones assessed using *KJHH*, tends to give higher $\mathrm{DPI}L_{ij}$ values. Before updating,

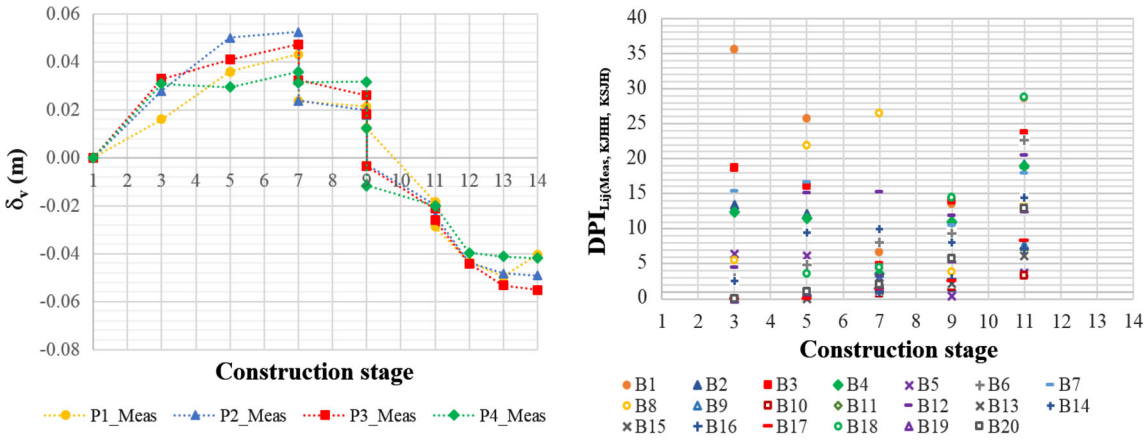

(a) Measured vertical displacements in monitoring points P1 to P4. Data from Cuevas (2012)

(b) *DPI* values for neighboring buildings B1 to B20 estimated using *KJHH*, *KSJH,* and measurements

Fig. 11 Vertical displacement measurements and assessed DPI values

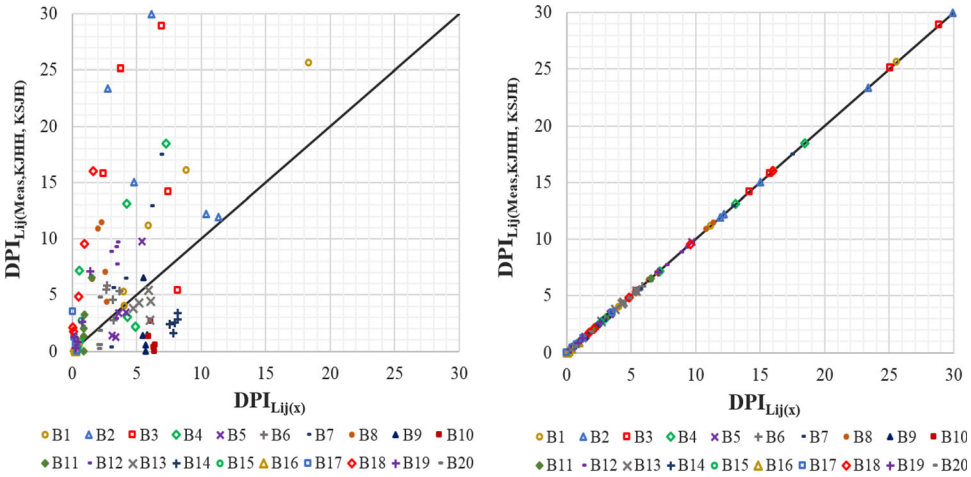

(a) Before updating

(b) After updating

Fig. 12 DPIL_{ij} values based on field measurements and *KJHH-KSJH* models versus mean DPIL_{ij} values based on *RSM*

58% of DPI predicted values from semiempirical models *KJHH-KSJH* including actual measurements were higher than those from nodal values in numerical analysis, 11% in construction stage 3, 4% in CS5, 12% in CS7, 14% in CS9 and 17% in CS11. As seen in Fig. 12, after updating, there is a good match among the estimated DPIL_{ij} values by the two approaches. These updated DPIL_{ij} mean values and obtained standard deviations were used to calculate posterior damage probabilities.

Figure 13 displays the estimated prior and posterior damage probabilities in neighboring buildings, in the second case only for the excavation stages in the constructive process. As most of $\mathrm{DPI}_{Lij(KJHH\text{-}KSJH)}$ values were higher than $\mathrm{DPI}_{Lij}(x)$ ones, when updating damage probability estimates, the posterior P''_{dij} will tend to increase compared to prior P'_{dij}. Considering only the excavation stages, the expected levels of performance are above average or better in 76% of analyzed cases after updating, while before updating they were 86%.

When considering updated damage probabilities for each building separately, B5, B9, B10, B11, B13, B14, B15, B16, B17, B19, B20, have a good performance ($0.001 < Pd_{ij} < 0.00003$) in at least 80% of the cases; for B6, 60% of the analyzed cases are above average ($0.001 < Pd_{ij} < 0.006$). In B12, 40% of analyzed cases are above average or better, but 60% are below average ($0.006 < Pd_{ij} < 0.023$). In B8, 60% of analyzed cases are above average or better, but 40% have poor performance ($0.023 < Pd_i < 0.07$). In B18, 60% of analyzed cases have a good performance, but 20% are below average, and 20% are unsatisfactory. B4 and B7 behave above average or better in 60% of analyzed cases, but 40% have poor performance or worse. The buildings with most unfavorable performances are B1, B2, B3, where at least 60% of the

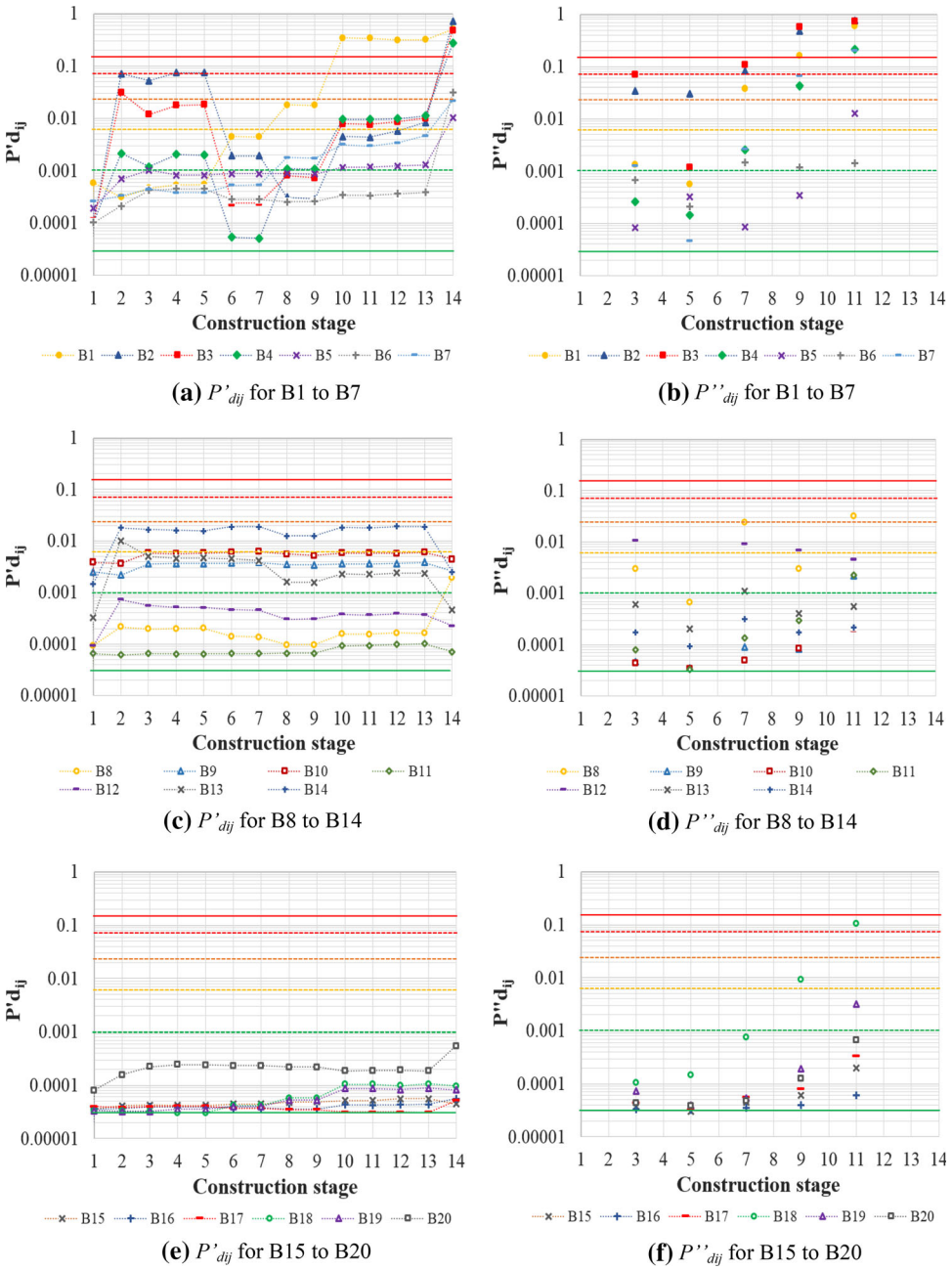

(a) P'_{dij} for B1 to B7 **(b)** P''_{dij} for B1 to B7

(c) P'_{dij} for B8 to B14 **(d)** P''_{dij} for B8 to B14

(e) P'_{dij} for B15 to B20 **(f)** P''_{dij} for B15 to B20

Fig. 13 Estimated prior P'_{dij} and posterior P''_{dij} damage probabilities in adjoining buildings to the considered synthetic excavation in CDMX soft soils

cases evidence a poor performance or worse, and 40% are hazardous ($Pd_{ij} > 0.16$).

As mentioned previously, estimated damage probabilities after Bayesian updating are higher than the assessed initially, because of the underestimation of ground movements in numerical and probabilistic analyses, giving rise to lower DPI_L values. However, the obtained P''_{dij} values were in some cases lower than assessed P'_{dij} values, particularly at construction stage 7. $\mu P''_{dij}$ were 2.94 times $\mu P'_{dij}$ for construction stage 3 and 0.77 times $\mu P'_{dij}$ for construction stage 5, but reach much higher values as 39.1 times for construction stage 7, 138 times for construction stage 9 and 85 times for construction stage 11. As a result, the qualitative distribution of assessed damage probability values also changes after updating as shown in Fig. 14.

Bayesian updating also causes a reduction in the uncertainty of random parameters E_0^{ref} and E_{50}^{ref}, as shown in Fig. 15. While the mean values of E_0^{ref} and E_{50}^{ref} remained unchanged after updating, posterior standard deviation values were around 16% and 12% of prior values, respectively. In this case, $\mu_{\mathrm{DPI}L}$ values tend to reduce around a 25%, and the narrowing of E_0^{ref} and E_{50}^{ref}

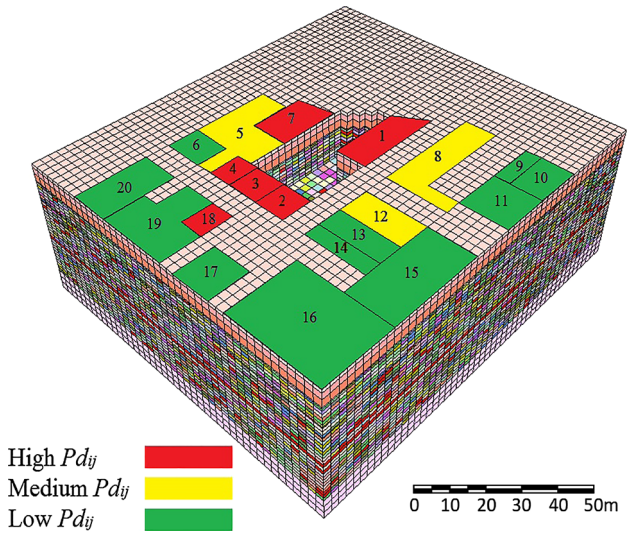

Fig. 14 Qualitative distribution of assessed Pd_{ij} values in RNDF-based models after Bayesian updating

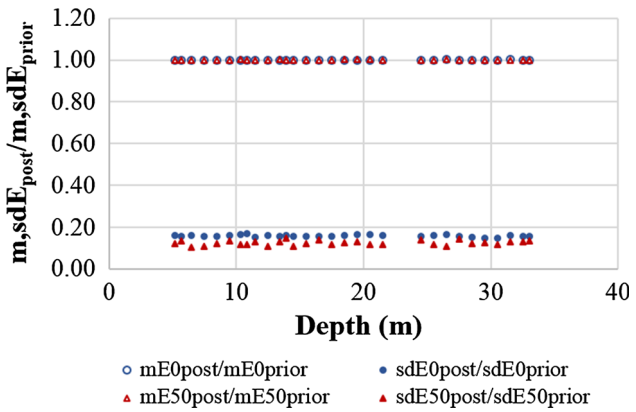

Fig. 15 Change in mean and standard deviation values for E_{0ref} and E_{50}^{ref} after Bayesian updating

distributions also caused a reduction in σ_{DPIL} because after updating, σ_{DPIL} was 0.21 times its initial value. When recalculating prior damage probabilities using the new μ_{DPIL} and σ_{DPIL} values, they were 0.51 to 0.59 times the ones presented and discussed in the previous section.

Conclusions

In this case, when comparing random field and random variable-based model results, despite having similar trends across the construction process, the assessed Pd_{ij} values are different for the two representations of soil parameter variability. The assessed damage probabilities are higher for random field-based models, and when considering results for all buildings, the average differences in Pd_{ij} values are around 60%. The qualitative distributions of assessed damage probabilities, established to visualize potential damages, also show different potential damage distributions in the buildings located around the excavation when changing the soil variability representation.

The Pd_{ij} obtained results are similar when using Gaussian and Pearson's type I-Beta distributions for random parameters E_0^{ref} and E_{50}^{ref} in *RSM* polynomial equations. In results for all buildings, the differences in Pd_{ij} are on average around 25% for random field-based models and 6% for random variable-based models. On the other hand, when comparing *RSM* and *PEM* results using Gaussian distribution of random parameters, the Pd_{ij} values are also similar. Regarding results for all buildings, the differences in Pd_{ij} are on average around 14% for random field-based models and around 2% for random variable-based models.

Bayesian updating was used in this paper to combine information from semiempirical methods and actual measurements with numerical and probabilistic analyses in order to enhance initially obtained performance predictions. The updating was performed on DPI_L values calculated from polynomial equations obtained through *RSM*. Once analyzed the numerical models, the application of *RSM* is more laborious compared to *PEM* because it implies finding the coefficients β_i of polynomial equations. However, using *RSM* is more advantageous because the polynomial equations defined for each building and construction stage can be used for the prediction performance updating.

In this case, numerical and probabilistic analyses underestimate the modeled system performance, delivering lower DPI_L values than the ones obtained when combining semiempirical methods and actual measurements. As a result when updating damage probability estimates, the posterior P''_{dij} tends to increase considerably compared to prior P'_{dij}, and the qualitative distribution of assessed damage probability values changes. Besides, the Bayesian updating also causes a reduction in the uncertainty of random parameters E_0^{ref} and E_{50}^{ref}, causing a reduction in calculated μ_{DPIL} and σ_{DPIL} when using the polynomial equations from *RSM*.

Acknowledgements The first author also acknowledges support and guidance from Dr. Auvinet and researchers of Laboratorio de Geoinformática, Instituto de Ingeniería, UNAM.

Funding This research project had funds from Doctoral Grant 617 provided by Colciencias and Universidad Nacional de Colombia and project 28394 Hermes-Universidad Nacional de Colombia. Universidad Pedagógica y Tecnológica de Colombia supported the first author by conceding the Doctoral Study Commission 199-2014.

Compliance with Ethical Standards

Conflict of interest The authors declare that they have no conflict of interest.

References

1. Kempfert HG, Gebreselassie B (2006) Excavations and foundations in soft soils. Springer, Berlin
2. Marsal RJ, Mazari M (2016) The subsoil of Mexico City, 3rd edn, vol I, II. Instituto de Ingeniería Universidad Nacional Autónoma de México, 456 p, Vol I, 366 p, Vol II
3. Auvinet G, Méndez E, Juárez M (2016) The subsoil of Mexico City, vol III, 3rd edn. Instituto de Ingeniería Universidad Nacional Autónoma de México, CDMX
4. Auvinet G (2017) Sixty years of geotechnical engineering in Mexico (1957–2017). In: 4th international conference on deep foundations SMIG, DFI, ASCE G-I, ISSMGE TC-214. SMIG, Mexico City, pp xv–xxxvii
5. Díaz-Rodríguez JA (2003) Characterization and engineering properties of Mexico City lacustrine soils. In: Tan TS et al (eds) Characterization and engineering properties of natural soils. Swets & Zeitlinger, Lisse, pp 725–755
6. Ovando-Shelley E (2011). Some geotechnical properties to characterize Mexico City Clay. In: Proceedings 14th Pan-am CGS Geotechnical Conference. Canadian Geotechnical Society, Toronto, Canada, 12 p
7. Juárez M (2015) Análisis Geoestadístico del Subsuelo de la Zona Lacustre del Valle de México. México, D.F. Tesis Doctoral, Universidad Nacional Autónoma de México, 426 p
8. Juárez-Camarena M, Auvinet-Guichard G, Méndez-Sánchez E (2016) Geotechnical zoning of Mexico Valley subsoil. Ingeniería, Investigación y Tecnología 17(3):297–308
9. Auvinet G, Romo-Organista M (1998) Deep excavations in Mexico City soft clays. In: Symposium on Big Digs Around the World, ASCE National Convention. Boston, Massachusetts: ASCE Special Publication No 86, pp 211–229
10. Zeevaert L (1957) Foundation design and behavior of Tower Latino Americana in Mexico City. Géotechnique 6:115–133
11. Vera AV, Gonzalez GM, Gonzalez LB, Gomez AS, Vara JM (1995) Twenty-five years of subway construction in Mexico City. Tunn Undergr Sp Tech 10(1):65–77
12. Auvinet G (2014) Comportamiento del Sistema de Transporte Colectivo (Metro) de la Ciudad de México en presencia de hundimiento regional. XIV CCG & IVSAYGEC. Sociedad Colombiana de Geotecnia, Bogotá DC, pp 16–30
13. Paulín-Aguirre J (2014) Panorama actual de las excavaciones profundas en las arcillas blandas del Valle de México. XIV CCG & IVSAYGEC. Sociedad Colombiana de Geotecnia, Bogotá DC, pp 222–233
14. GCDMX (2017) Normas Técnicas Complementarias para Diseño y Construcción de Cimentaciones. Gaceta Oficial de la Ciudad de México No 220 Bis. Gobierno de la Ciudad de México, CDMX, 712 p
15. Korff M (2009) Deformations and damage to buildings adjacent to deep excavations in soft soils. Deltares, Delft, p 136
16. Ahmed SM (2014) State-of-the-art report: deformations associated with deep excavation and their effects on nearby structures. Ain Shams University, Cairo, p 164
17. Schanz T, Vermeer PA, Bonnier PG (1999) The hardening soil model: formulation and verification. In: Beyond 2000 in Computational Geotechnics—10 years of PLAXIS. Balkema, Rotterdam, pp 1–16
18. Benz T (2007) Small-strain stiffness of soils and its numerical consequences. Institut für Geotechnik der Universität Stuttgart, 193 p
19. Obrzud RF (2010) On the use of the Hardening Soil Small Strain model in geotechnical practice. Numerics in Geotechnics and Structures. Elmepress International, Lausanne, pp 15–32
20. Obrzud R, Truty A (2014) The hardening soil model—a practical guidebook, Z_Soil.PC 100701 Report revised 31.09.2014. Zace Services Ltd., Lausanne, 205 p
21. Auvinet G (2002) Uncertainty in geotechnical engineering. In: Sixteenth Nabor Carrillo Lecture—XXIth National Meeting of the Mexican Society of Soil Mechanics. SMIG, Querétaro, pp 1–139
22. Baecher GB, Christian JT (2003) Reliability and statistics in geotechnical engineering. Wiley, Hoboken
23. Nadim F, Einstein H, Roberds W (2005) Probabilistic stability analysis for individual slopes in soil and rock. In: Landslides risk management. Taylor & Francis Group, pp 63–98
24. Sánchez M (2010) Introducción a la confiabilidad y evaluación de riesgos. Teoría y aplicaciones en ingeniería. Segunda Edición. Facultad de Ingeniería Universidad de Los Andes, Bogotá, DC, 457 p
25. Straub D (2014) Engineering risk assessment. In: Risk—a multidisciplinary introduction. Springer, Berlin, pp 333–362
26. Schuster M (2008) Framework for the fully probabilistic analysis of excavation-induced serviceability damage to buildings in soft clays. All Dissertations, Clemson University, 141 p
27. Schuster M, Kung GT, Hsein Juang C, Hashash YM (2009) Simplified model for evaluating damage potential of buildings adjacent to a braced excavation. J Geotech Geoenviron 135(12):1823–1835
28. Cuevas A (2012) Diseño de Sistemas de Contención para Excavaciones. Tesis de Maestría, Universidad Nacional Autónoma de México, México D.F., 168 p
29. Kung GT, Hsein Juang C, Hsiao EC, Hashash YM (2007) Simplified model for wall deflection and ground-surface settlement caused by braced excavation in clays. J Geotech Geoenviron 133(6):731–747
30. Uzielli M, Lacasse S, Nadim F, Phoon K-K (2006) Soil variability analysis for geotechnical practice. In: Proceedings of the 2nd international workshop on characterisation and engineering properties of natural soils, Singapore, pp 1653–1754
31. Jaksa MB (2007) Modeling the natural variability of over-consolidated clay in Adelaide, South Australia. In: Characterization and engineering properties of natural soils. Taylor & Francis Group, pp 2721–2752
32. Fenton GA, Griffiths DV (2008) Risk assessment in geotechnical engineering. Wiley, Hoboken
33. Huber M (2013) Soil variability and its consequences in geotechnical engineering. Doctoral Dissertation, Institut für Geotechnik Universität Stuttgart, 272 p
34. Phoon K-K, Prakoso WA, Wang Y, Ching J (2016) Uncertainty representation of geotechnical design parameters. In: Reliability of geotechnical structures in ISO2394. CRC Press, pp 49–88
35. Ching J, Wu T-J, Stuedlein AW, Bong T (2018) Estimating horizontal scale of fluctuation with limited CPT soundings. Geosci Front 9:1597–1608
36. Elkateb T, Chalaturnyk R, Robertson P (2003) An overview of soil heterogeneity: quantification and implications on geotechnical field problems. Can Geotech J 40(1):1–15
37. Onyejekwe S, Kang X, Ge L (2016) Evaluation of the scale of fluctuation of geotechnical parameters by autocorrelation function and semivariogram function. Eng Geol 214:43–49
38. Rackwitz R (2000) Reviewing probabilistic soils modelling. Comput Geotech 26:199–223
39. Emery X (2013) Geoestadística. Facultad de Ciencias Físicas y Matemáticas Universidad de Chile, Santiago de Chile
40. Olea RA (2017) A practical primer on geostatistics, Open-File Report 2009-1103, Version 1.3. U.S. Geological Survey, 346 p
41. Remy N, Boucher A, Wu J (2009) Applied geostatistics with SGeMS. Cambridge University Press, Cambridge

42. Bakker KJ (2006) A 3D FE model for excavation analysis. In: Bakker et al (eds) Geotechnical aspects of underground construction in soft ground. Taylor & Francis Group, London, pp 473–478
43. Finno RJ, Blackburn JT, Roboski JF (2007) Three-dimensional effects for supported excavations in clay. J Geotech Geoenviron 133(1):30–36
44. Son M, Cording EJ (2005) Estimation of building damage due to excavation-induced ground movements. J Geotech Geoenviron 131(2):162–177
45. Duncan JM, Sleep MD (2015) Evaluating reliability in geotechnical engineering. In: Risk and reliability in geotechnical engineering. CRC Press, pp 131–179
46. Low B-K (2015) Reliability-based design: practical procedures, geotechnical examples. In: Risk and reliability in geotechnical engineering. CRC Press, pp 355–394
47. Bucher CG, Bourgund U (1990) A fast and efficient response surface approach for structural reliability problems. Struct Saf 7(1):57–66
48. Myers RH, Montgomery DC, Anderson-Cook CM (2016) Response surface methodology. Process and product optimization using designed experiments, 4th edn. Wiley, Hoboken
49. Rosenblueth E (1975) Point estimates for probability moments. Proc Natl Acad Sci USA 72(10):3812–3814
50. Idris MA, Nordlund E, Saiang D (2016) Comparison of different probabilistic methods for analyzing slope stability of underground rock excavations. Electron J Geotech Eng 21:6555–6585
51. Zhang J, Chen HZ, Huang HW, Luo Z (2015) Efficient response surface method for practical geotechnical reliability analysis. Comput Geotech 69:496–505
52. Li D-Q, Zheng D, Cao Z-J, Tang X-S, Phoon K-K (2016) Response surface methods for slope reliability analysis: review and comparison. Eng Geol 203:3–14
53. Nowak AS, Collins KR (2000) Reliability of structures. Mc Graw Hill, Boston
54. Hsein Juang C, Schuster M, Ou CY, Phoon K-K (2011) Fully probabilistic framework for evaluating excavation-induced damage potential of adjacent buildings. J Geotech Geoenviron 137(2):130–139
55. Wu TH (2009) Reliability of geotechnical predictions. In: Geotechnical risk and safety. Taylor & Francis Group, pp 3–10
56. Hsein Juang C, Luo Z, Atamturktur S, Huang H (2013) Bayesian updating of soil parameters for braced excavations using field observations. J Geotech Geoenviron 39(3):395–406
57. Straub D, Papaioannou I (2015) Bayesian analysis for learning and updating geotechnical parameters and models with measurements. In: Risk and reliability in geotechnical engineering. CRC Press, pp 221–264
58. Baecher GB (2017) Bayesian thinking in geotechnics Bayesian thinking in geotechnics. In: Second Suzanne Lacasse Lecture of the ISSMGE. Proceedings of GeoRisk2017. American Society of Civil Engineers, Denver, pp 1–19
59. Qi X-H, Zhou WH (2017) An efficient probabilistic back-analysis method for braced excavations using wall deflection data at multiple points. Comput Geotech 85:186–198
60. US Army Corps of Engineers (1997) Engineering and design introduction to probability and reliability methods for use in geotechnical engineering. Technical Letter No. 1110-2-547. Department of the Army, Washington, D.C., 168 p
61. Lunn D, Jackson C, Best N, Thomas A, Spiegelhalter D (2012) The BUGS book, a practical introduction to Bayesian analysis. CRC Press, Boca Raton
62. Krushke JK (2015) Doing Bayesian data analysis: a tutorial with R, JAGS, and Stan, 2nd edn. Academic Press, Cambridge